Variations in the long-term uplift rate due to the Altiplano-Puna Magma Body observed with Sentinel-1 interferometry

Homan Lau, Ekaterina Tymofyeyeva, Yuri Fialko

Institute of Geophysics and Planetary Physics, Scripps Institution of Oceanography, University of California, San Diego, La Jolla, CA 92093, USA.

Abstract

We present new Interferometric Synthetic Aperture Radar (InSAR) observations of surface deformation in the Altiplano-Puna region (South America) where previous studies documented a broad uplift at an average rate of ∼10 mm/year. We use data from the Sentinel-1 satellite mission to produce high-resolution velocity maps and time series of surface displacements between years 2014-2017. The data reveal that the uplift has slowed down substantially compared to the 1992-2010 epoch and is characterized by short-term fluctuations on time scales of months to years. The observed variations in uplift rate may indicate a non-steady supply of melt and/or volatiles from the partially molten Altiplano-Puna Magma Body (APMB) into an incipient diapir forming in the roof of the APMB.

Keywords: Altiplano, magma, diapir, uplift, InSAR

1. Introduction

The Altiplano-Puna plateau in the Andes (South America) hosts one of the world's largest and most active volcanic provinces, the Altiplano-Puna Volcanic Complex (APVC), which spans southern Bolivia, northern Chile, and northern Argentina, and includes more than 50 potentially active volcanos (e.g., Silva 1989). Seismic observations have detected a large low-velocity anomaly in the mid-to-upper crust underneath the APVC referred

Email address: h4lau@ucsd.edu ()

Published in Earth and Planetary Science Letters, 491:43-47, 2018

to as the Altiplano-Puna Ultra-Low Velocity Zone (APULVZ) (Chmielowski et al. 1999; Zandt et al. 2003; Ward et al. 2017). The observed reduction in seismic velocities requires the presence of partial melt, making the APULVZ the largest known active magma body in the Earth's continental crust. Space geodetic observations revealed a ∼75 km-wide zone of surface uplift in the middle of the APULVZ, with a peak near the dormant Uturuncu volcano (Pritchard and Simons 2002; Sparks et al. 2008). Fialko and Pearse (2012) showed that the uplift occurred at a quasi-constant rate of ∼10 mm/yr between 1992 and 2010, and was surrounded by a broad zone of subsidence occurring at a rate of a few mm/yr - an unusual pattern referred to as the "sombrero uplift". Gottsmann et al. (2017a) suggested that the uplifted persisted at the same rate over the last 50 years, based on leveling and campaign Global Positioning System (GPS) data.

Model-based interpretations of the observed surface deformation attribute the central uplift to a magmatic source in the middle crust at depth of ∼15-20 km (Fialko and Pearse 2012; Pritchard and Simons 2004; Henderson and Pritchard 2013; Hickey et al. 2013; Potro et al. 2013; Walter and Motagh 2014), although particular mechanisms of magmatic unrest are still not well-understood. Fialko and Pearse (2012) argued that the inferred mid-crustal depth of the deformation source, the proximity to the partially molten Altiplano-Puna Magma Body (APMB), and the long duration and quasi-steady nature of uplift imply viscous deformation mechanisms in the source region. One such mechanism could involve the formation and growth of a large magmatic diapir (Fialko and Pearse 2012). According to this model, the ballooning diapir causes the central uplift, while withdrawal of partial melt from the APMB into the diapir is responsible for the peripheral subsidence. The diapir model appears to be consistent with recent seismic (Jay et al. 2012; Ward et al. 2014), gravity (Potro et al. 2013), and electromagnetic (Comeau et al. 2016; Laumonier et al. 2017) observations, as well as earlier suggestions that large amounts of dacite melt may be transported in diapirs from the middle to the upper crust within the APVC proper (Silva 1989). Gottsmann et al. (2017b) presented data from a continuous GPS site installed in 2010 near the center of uplift, showing variations in the uplift rate on sub-decadal time scales, and proposed that the observed surface deformation may result from cycles of pressurization and de-pressurization in a vertically-elongated magma reservoir connected to the APMB, similar to the incipient diapir geometry inferred by Fialko and Pearse (2012).

In this paper, we present new Interferometric Synthetic Aperture Radar

(InSAR) data that extend the time series of surface deformation in Altiplano-Puna to 25 years. The new observations reveal that the uplift rate has decreased over the last decade compared to the previous two decades, and that the rates of surface motion may indeed fluctuate on time scales on the order of months to years. We discuss implications from the observed time history of uplift for possible driving mechanisms.

2. Data and Methods

We analyzed data acquired between September 2014 and December 2017 by the Sentinel-1A/B satellites. We used individual sub-swaths from ascending tracks 76, 149 and descending tracks 83, 156 (Figure 1), covering the area of uplift imaged by the ERS-1/2 and Envisat observations between the years 1992 and 2010 (Pritchard and Simons 2002; Fialko and Pearse 2012; Henderson and Pritchard 2013). The data were processed using the Generic Mapping Tools Synthetic Aperture Radar (GMTSAR) package (Sandwell et al. 2011). We produced interferograms for every pair of sequential acquisitions for each satellite track, resulting in a total of 215 interferometric pairs (see Figures S1 and S2 of Supporting Information). Single look complex images were aligned using the Bivariate Enhanced Spectral Diversity (BESD) method (Wang et al. 2017). We used the Shuttle Radar Topography Mission (SRTM) 30m resolution digital elevation model (DEM) (Farr and Kobrick 2000) to remove the topographic contribution from the interferometric phase. Interferograms were unwrapped using the SNAPHU algorithm (Chen and Zebker 2002). Short revisit times and tight orbital controls of the Sentinel-1 satellites, combined with arid low-vegetation surface conditions, result in high coherence of interferometric phase in the study area.

Propagation effects are known to be the main limitation to the accuracy of InSAR measurements of low-amplitude deformation (Tarayre and Massonnet 1996; Fialko and Simons 2001; Li et al. 2005; Foster et al. 2006; Ding et al. 2008). In particular, interferometric phase can be affected by variations in the electron content in the ionosphere, and water vapor in the troposphere. Tropospheric contributions consist in part of a turbulent component that is random in time and follows a power law distribution in space (e.g., Ding et al. 2008), and a stratified component that may or may not be systematic in time but is spatially correlated with topography (e.g., Doin et al. 2009). We estimated the propagation effects due to ionosphere and turbulent water vapor mixing in the troposphere using an iterative common-scene stacking method

CANDIS (Tymofyeyeva and Fialko 2015). The method takes advantage of frequent data acquisitions to estimate and remove the propagation artifacts, under the assumption of quasi-constant rates of surface deformation. The temporally random component of phase delays was calculated using a 200-day averaging stencil (see Tymofyeyeva and Fialko 2015, for details). Figures S1 and S2 in Supporting Information show the estimated atmospheric noise coefficients (a measure of the amplitude of propagation artifacts) for different acquisition dates.

After we applied the CANDIS correction, some interferograms exhibited a correlation between the unwrapped radar phase and topography, which could be attributed to residual propagation delays due to a stratified troposphere. These signals can vary systematically with time (e.g., due to seasonal variations in tropospheric water content), in which case they would not be removed by the common-point stacking method, as the latter preserves any variations in phase that are quasi-linear on a time scale of satellite revisits. To mitigate the seasonally-varying atmospheric noise, we combined sequential interferograms (corrected for the turbulent noise) to form a set of year-long interferograms that begin and end on the same month of a year. This resulted in $\sim$20 independent year-long interferograms for each track. We found that addition of sequential interferograms may introduce a high-frequency noise to the radar phase due to filtering artifacts. Therefore filtering and unwrapping were applied after summation of individual raw interferograms. Interferograms with a time span of one year minimize seasonal differences in the net water vapor content in the troposphere, although may still be affected by longer-term (e.g. decadal) trends. Each one-year interferogram was subsequently "de-ramped", by subtracting the best-fit plane, to correct for any residual long-wavelength artifacts. We then estimated the remaining contributions due to the stratified water vapor in the atmosphere by regressing the line of sight (LOS) displacements against elevation (e.g., Bekaert et al. 2015). To prevent a potential bias due to surface deformation, we excluded data from the geodetically imaged uplift area (black dashed circle in Figure 1). The observed dependence of LOS displacements on topography is illustrated in Figure S3. After subtracting the best-fit linear scaling between phase and topography from the year-long interferograms, we computed the mean LOS velocities by averaging the corrected year-long interferograms for each track and dividing by the respective time interval. Averaging is expected to further suppress any residual random noise by a factor of $\sqrt{N}$ given N independent samples (e.g., Zebker et al. 1997; Fialko 2006). The results are shown in Fig-

ure 2. We also computed time series of LOS displacements from the original set of sequential interferograms corrected for the turbulent atmospheric noise (Tymofyeyeva and Fialko 2015).

3. Results

Figure 3 shows a profile of the mean LOS velocities from the four Sentinel-1 tracks spanning the uplift area (Figure 2). For comparison, we also include the mean LOS velocities from the same profile corresponding to the previous ∼20 years (1992-2010; pink dots in Figure 3). While the LOS velocities derived from Sentinel-1 data are still noisy because of the relatively short observation period, they consistently indicate that the uplift rate over the last 3 years is considerably decreased compared to the average uplift rate over the previous 20 years. The peak uplift rate constrained by Sentinel-1 observations is 3–5 mm/year (Figure 3), which is a factor of 2 to 3 smaller than the average rates documented between 1992-2010 (Fialko and Pearse 2012; Pritchard and Simons 2004; Henderson and Pritchard 2013).

To get a further insight into the details of uplift history, we compiled the 25-year-long time series of LOS displacements at the center of uplift, combining previously published ERS-1/2 and ENVISAT (Fialko and Pearse 2012), continuous GPS (Gottsmann et al. 2017b), and new Sentinel-1 data (Figure 4). A close-up view of the last several years of deformation is presented in Figure S4 in the Supporting Information. The data indicate a gradual decrease in the uplift rate over the observation time period, punctuated by short-term (sub-decadal to sub-annual) fluctuations. The timeseries shown in Figure 4 may also indicate that the long-term uplift accelerated during 1998-2003, and then returned to a quasi-steady average rate of 5-8 mm/yr.

The Sentinel-1 timeseries of LOS displacements clearly show that the vertical component of surface velocity at the center of uplift is not constant and may even exhibit short-term small-amplitude reversals (i.e., subsidence). Such fluctuations may also be seen in the ENVISAT data during periods of sufficiently frequent acquisitions (Figure 4). That the LOS displacements are indicative of a predominantly vertical motion follows from the agreement between the InSAR data from different lines of sight (Figure S4) (Lundgren et al. 2003; Fialko et al. 2005). The Sentinel-1 measurements also reveal a localized zone of subsidence to the south of the Uturuncu volcano (see red outline in (Figure 2) at a rate of ∼9 mm/year. The estimated source depth

of 2.12 km (see Supporting Information) suggests that this subsidence might be due to a shallow hydrothermal system.

The new InSAR data do not clearly show the ring of subsidence around the uplift (Figure 2). Assuming that the rate of flanking subsidence is proportional to the rate of uplift, the "sombrero" pattern is likely below the noise level of the available 2014-2017 InSAR data.

4. Discussion

The non-steady nature of deformation near Uturuncu revealed by space geodetic observations (Figure 4) has implications for the mechanisms driving the uplift. Numerical models of a buoyant diapir forming in the roof of the partially molten Altiplano-Puna Magma Body do predict gradual decreases in the uplift rate with time (Fialko and Pearse 2012). Episodic acceleration or deceleration of uplift could possibly be attributed to variations in magma supply from the partially molten APMB to the diapir, given likely spatial and temporal variations in the effective permeability and viscosity within the APMB. This interpretation is supported by the observed spatial variations in the rate of subsidence surrounding the central uplift (Fialko and Pearse 2012; Henderson and Pritchard 2013). However, the diapir models cannot readily explain the short-term velocity reversals that appear to be well resolved by recent observations (Figures 4 and S4).

Gottsmann et al. (2017b) argued that variations in the uplift rate are inconsistent with "en masse diapiric ascent of material from the APMB toward the surface", and instead proposed that the observed surface deformation reflects pressure changes due to migration of volatiles and/or melt in a vertically-elongated magma body connected to the APMB. We point out that the models of Fialko and Pearse (2012) and Gottsmann et al. (2017b) are not mutually exclusive. Indeed, the existence of a molten or partially molten vertical column on top of the APMB postulated by Gottsmann et al. (2017b) can naturally result from the Rayleigh-Taylor instability driven by the density contrasts (Fialko and Pearse 2012; Bittner and Schmeling 1995). Inversely, the low density of material in such a column (Potro et al. 2013) necessarily implies a buoyant force and viscous response of the hot ambient crust. The main difference between the proposed models is the relative importance of volatiles (with respect to melt) in the presumed mass transfer between the APMB and the vertically elongated reservoir in its roof. Gottsmann et al. (2017b) suggested that both the long-term uplift and the short-term fluctu-

ations in the rate of vertical motion can be explained by pressurization and de-pressurization (due to volatile loss) of the vertically elongated extension of the APMB. Alternatively, the diapir model implies that the long-term uplift is primarily due to melt migration, while the short-term fluctuations could be caused by local magma intrusions or migration of volatiles. The model of Gottsmann et al. (2017b) further implies that the observed uplift will be followed by subsidence with amplitude comparable to that of the observed uplift, i.e., hundreds of millimeters. The hypothesized subsidence should occur at a rate that is controlled by degassing, which can be relatively fast judging by the rates of short-term variations in the observed surface motion (tens of millimeters per year, Figures 4). On the contrary, the diapir model (Fialko and Pearse 2012) predicts no significant future subsidence on timescales of years to centuries. Thus the role of volatiles in the observed deformation can be potentially evaluated with long-term monitoring.

5. Conclusions

We presented InSAR data collected by the Sentinel-1 mission between 2014-2017, extending the time series of surface deformation in Altiplano-Puna to 25 years. The average uplift rate has decreased over the last decade compared to the average uplift rate over the previous two decades documented by previous studies. Additionally, the data indicate that the rates of surface motion can fluctuate on time scales of months to years. We attribute the observed changes in the uplift rate to variations in melt supply from the APMB to a large diapir forming in the roof of the APMB. Migration and subsequent loss of volatiles may be responsible for the observed short-term, small-amplitude fluctuations in the rate of surface motion. Continued observations of magmatic unrest in Altiplano at high spatial and temporal resolution will further improve our understanding of the dynamics of large-midcrustal magma bodies, as well as the mechanisms of magma transport through the Earth's crust.

Acknowledgments

This study was supported by NASA (grant NNX14AQ15G). Sentinel-1 data were provided by the European Space Agency (ESA) through Alaska Satellite Facility (ASF) and UNAVCO. Figures 1 and 2 were generated using the Generic Mapping Tools (GMT) (Wessel et al. 2013). Data used in this study are available at `http://igppweb.ucsd.edu/~fialko/data.html`.

References

S. L. d. Silva, Altiplano-Puna volcanic complex of the central Andes, Geology 17 (12) (1989) 1102–1106, ISSN 0091-7613, 1943-2682, doi:\bibinfo{doi}{10.1130/0091-7613(1989)017⟨1102:APVCOT⟩2.3.CO;2}, URL http://geology.gsapubs.org/content/17/12/1102.

J. Chmielowski, G. Zandt, C. Haberland, The Central Andean Altiplano-Puna magma body, Geophys. Res. Lett. 26 (6) (1999) 783–786, ISSN 1944-8007, doi:\bibinfo{doi}{10.1029/1999GL900078}, URL http://onlinelibrary.wiley.com/doi/10.1029/1999GL900078/abstract.

G. Zandt, M. Leidig, J. Chmielowski, D. Baumont, X. Yuan, Seismic Detection and Characterization of the Altiplano-Puna Magma Body, Central Andes, in: Y. Ben-Zion (Ed.), Seismic Motion, Lithospheric Structures, Earthquake and Volcanic Sources: The Keiiti Aki Volume, Pageoph Topical Volumes, Birkhuser Basel, ISBN 978-3-7643-7011-4 978-3-0348-8010-7, 789–807, dOI: 10.1007/978-3-0348-8010-7_14, 2003.

K. M. Ward, J. R. Delph, G. Zandt, S. L. Beck, M. N. Ducea, Magmatic evolution of a Cordilleran flare-up and its role in the creation of silicic crust, Scientific Reports 7 (1) (2017) 9047, ISSN 2045-2322, doi:\bibinfo{doi}{10.1038/s41598-017-09015-5}, URL https://www.nature.com/articles/s41598-017-09015-5.

M. E. Pritchard, M. Simons, A satellite geodetic survey of large-scale deformation of volcanic centres in the central Andes, Nature 418 (6894) (2002) 167–171, ISSN 0028-0836, doi:\bibinfo{doi}{10.1038/nature00872}, URL http://www.nature.com/nature/journal/v418/n6894/abs/nature00872.html.

R. S. J. Sparks, C. B. Folkes, M. C. S. Humphreys, D. N. Barfod, J. Clavero, M. C. Sunagua, S. R. McNutt, M. E. Pritchard, Uturuncu volcano, Bolivia: Volcanic unrest due to mid-crustal magma intrusion, American Journal of Science 308 (6) (2008) 727–769, ISSN 0002-9599, 1945-452X, doi:\bibinfo{doi}{10.2475/06.2008.01}, URL http://www.ajsonline.org/content/308/6/727.

Y. Fialko, J. Pearse, Sombrero Uplift Above the Altiplano-Puna Magma Body: Evidence of a Ballooning Mid-Crustal Diapir, Science 338 (6104)

(2012) 250–252, ISSN 0036-8075, 1095-9203, doi:\bibinfo{doi}{10.1126/science.1226358}, URL http://science.sciencemag.org/content/338/6104/250.

J. Gottsmann, R. del Potro, C. Muller, 50 years of steady ground deformation in the Altiplano-Puna region of southern Bolivia, Geosphere 14 (2017a) 65–73.

M. E. Pritchard, M. Simons, An InSAR-based survey of volcanic deformation in the central Andes, Geochemistry, Geophysics, Geosystems 5 (2) (2004) Q02002, ISSN 1525-2027, doi:\bibinfo{doi}{10.1029/2003GC000610}, URL http://onlinelibrary.wiley.com/doi/10.1029/2003GC000610/abstract.

S. T. Henderson, M. E. Pritchard, Decadal volcanic deformation in the Central Andes Volcanic Zone revealed by InSAR time series, Geochemistry, Geophysics, Geosystems 14 (5) (2013) 1358–1374, ISSN 1525-2027, doi:\bibinfo{doi}{10.1002/ggge.20074}, URL http://onlinelibrary.wiley.com/doi/10.1002/ggge.20074/abstract.

J. Hickey, J. Gottsmann, R. del Potro, The large-scale surface uplift in the Altiplano-Puna region of Bolivia: A parametric study of source characteristics and crustal rheology using finite element analysis, Geochemistry, Geophysics, Geosystems 14 (3) (2013) 540–555, ISSN 1525-2027, doi:\bibinfo{doi}{10.1002/ggge.20057}, URL http://onlinelibrary.wiley.com/doi/10.1002/ggge.20057/abstract.

R. Potro, M. Díez, J. Blundy, A. G. Camacho, J. Gottsmann, Diapiric ascent of silicic magma beneath the Bolivian Altiplano, Geophys. Res. Lett. 40 (10) (2013) 2044–2048.

T. R. Walter, M. Motagh, Deflation and inflation of a large magma body beneath Uturuncu volcano, Bolivia? Insights from InSAR data, surface lineaments and stress modelling, Geophysical Journal International 198 (1) (2014) 462–473, ISSN 0956-540X, doi:\bibinfo{doi}{10.1093/gji/ggu080}, URL https://academic.oup.com/gji/article/198/1/462/602550/Deflation-and-inflation-of-a-large-magma-body.

J. A. Jay, M. E. Pritchard, M. E. West, D. Christensen, M. Haney, E. Minaya, M. Sunagua, S. R. McNutt, M. Zabala, Shallow seismic-

ity, triggered seismicity, and ambient noise tomography at the long-dormant Uturuncu Volcano, Bolivia, Bulletin of Volcanology 74 (4) (2012) 817–837, ISSN 0258-8900, 1432-0819, doi:\bibinfo{doi}{10.1007/s00445-011-0568-7}, URL https://link.springer.com/article/10.1007/s00445-011-0568-7.

K. M. Ward, G. Zandt, S. L. Beck, D. H. Christensen, H. McFarlin, Seismic imaging of the magmatic underpinnings beneath the Altiplano-Puna volcanic complex from the joint inversion of surface wave dispersion and receiver functions, Earth Planet. Sci. Lett. 404 (2014) 43–53.

M. J. Comeau, M. J. Unsworth, D. Cordell, New constraints on the magma distribution and composition beneath Volcán Uturuncu and the southern Bolivian Altiplano from magnetotelluric data, Geosphere 12 (5) (2016) 1391–1421.

M. Laumonier, F. Gaillard, D. Muir, J. Blundy, M. Unsworth, Giant magmatic water reservoirs at mid-crustal depth inferred from electrical conductivity and the growth of the continental crust, Earth Planet. Sci. Lett. 457 (2017) 173–180.

J. Gottsmann, J. Blundy, S. Henderson, M. Pritchard, R. Sparks, Thermomechanical modeling of the Altiplano-Puna deformation anomaly: Multiparameter insights into magma mush reorganization, Geosphere 13 (4) (2017b) 1042, doi:\bibinfo{doi}{10.1130/GES01420.1}, URL http://dx.doi.org/10.1130/GES01420.1.

D. Sandwell, R. Mellors, X. Tong, M. Wei, P. Wessel, Open radar interferometry software for mapping surface Deformation, Eos, Transactions American Geophysical Union 92 (28) (2011) 234–234, ISSN 2324-9250, doi:\bibinfo{doi}{10.1029/2011EO280002}, URL http://onlinelibrary.wiley.com/doi/10.1029/2011EO280002/abstract.

K. Wang, X. Xu, Y. Fialko, Improving burst alignment in TOPS interferometry with bivariate enhanced spectral diversity (BESD), IEEE Geoscience and Remote Sensing Letters 14 (2017) 2423–2427.

T. Farr, M. Kobrick, Shuttle Radar Topography Mission produces a wealth of data, AGU Eos 81 (2000) 583–585.

C. W. Chen, H. A. Zebker, Phase unwrapping for large SAR interferograms: Statistical segmentation and generalized network models, IEEE Transactions on Geoscience and Remote Sensing 40 (8) (2002) 1709–1719.

H. Tarayre, D. Massonnet, Atmospheric propagation heterogeneities revealed by ERS-1 interferometry, Geophys. Res. Lett. 23 (1996) 989–992.

Y. Fialko, M. Simons, Evidence for on-going inflation of the Socorro magma body, New Mexico, from Interferometric Synthetic Aperture Radar imaging, Geophys. Res. Lett. 28 (2001) 3549–3552.

Z. Li, J.-P. Muller, P. Cross, E. J. Fielding, Interferometric synthetic aperture radar (InSAR) atmospheric correction: GPS, Moderate Resolution Imaging Spectroradiometer (MODIS), and InSAR integration, Journal of Geophysical Research: Solid Earth 110 (B3) (2005) B03410, ISSN 2156-2202, doi:\bibinfo{doi}{10.1029/2004JB003446}, URL http://onlinelibrary.wiley.com/doi/10.1029/2004JB003446/abstract.

J. Foster, B. Brooks, T. Cherubini, C. Shacat, S. Businger, C. L. Werner, Mitigating atmospheric noise for InSAR using a high resolution weather model, Geophys. Res. Lett. 33 (16) (2006) L16304, ISSN 1944-8007, doi:\bibinfo{doi}{10.1029/2006GL026781}, URL http://onlinelibrary.wiley.com/doi/10.1029/2006GL026781/abstract.

X. Ding, Z. Li, J. Zhu, G. Feng, J. Long, Atmospheric Effects on InSAR Measurements and Their Mitigation, Sensors 8 (9) (2008) 5426–5448, doi:\bibinfo{doi}{10.3390/s8095426}, URL http://www.mdpi.com/1424-8220/8/9/5426.

M. P. Doin, C. Lasserre, G. Peltzer, O. Cavalié, C. Doubre, Corrections of stratified tropospheric delays in SAR interferometry: Validation with global atmospheric models, Journal of Applied Geophysics 69 (1) (2009) 35–50, ISSN 0926-9851, doi:\bibinfo{doi}{10.1016/j.jappgeo.2009.03.010}, URL http://www.sciencedirect.com/science/article/pii/S0926985109000603.

E. Tymofyeyeva, Y. Fialko, Mitigation of atmospheric phase delays in InSAR data, with application to the eastern California shear zone, Journal of Geophysical Research: Solid Earth 120 (8) (2015) 2015JB011886,

ISSN 2169-9356, doi:\bibinfo{doi}{10.1002/2015JB011886}, URL http://onlinelibrary.wiley.com/doi/10.1002/2015JB011886/abstract.

D. P. S. Bekaert, A. Hooper, T. J. Wright, A spatially variable power law tropospheric correction technique for InSAR data, Journal of Geophysical Research: Solid Earth 120 (2) (2015) 2014JB011558, ISSN 2169-9356, doi:\bibinfo{doi}{10.1002/2014JB011558}, URL http://onlinelibrary.wiley.com/doi/10.1002/2014JB011558/abstract.

H. A. Zebker, P. A. Rosen, S. Hensley, Atmospheric effects in interferometric synthetic aperture radar surface deformation and topographic maps, Journal of Geophysical Research: Solid Earth 102 (B4) (1997) 7547–7563, ISSN 2156-2202, doi:\bibinfo{doi}{10.1029/96JB03804}, URL http://onlinelibrary.wiley.com/doi/10.1029/96JB03804/abstract.

Y. Fialko, Interseismic strain accumulation and the earthquake potential on the southern San Andreas fault system, Nature 441 (2006) 968–971.

P. Lundgren, P. Berardino, M. Coltelli, G. Fornaro, R. Lanari, G. Puglisi, E. Sansosti, M. Tesauro, Coupled magma chamber inflation and sector collapse slip observed with synthetic aperture radar interferometry on Mt. Etna volcano, Journal of Geophysical Research: Solid Earth 108 (B5) (2003) 2247, ISSN 2156-2202, doi:\bibinfo{doi}{10.1029/2001JB000657}, URL http://onlinelibrary.wiley.com/doi/10.1029/2001JB000657/abstract.

Y. Fialko, D. Sandwell, M. Simons, P. Rosen, Three-dimensional deformation caused by the Bam, Iran, earthquake and the origin of shallow slip deficit, Nature 435 (2005) 295–299.

D. Bittner, H. Schmeling, Numerical Modelling of Melting Processes and Induced Diapirism In the Lower Crust, Geophysical Journal International 123 (1) (1995) 59–70, ISSN 0956-540X, doi:\bibinfo{doi}{10.1111/j.1365-246X.1995.tb06661.x}, URL https://academic.oup.com/gji/article/123/1/59/571293/Numerical-Modelling-of-Melting-Processes-and.

P. Wessel, W. H. F. Smith, R. Scharroo, J. Luis, F. Wobbe, Generic Mapping Tools: Improved Version Released, Eos, Transactions American Geophysical Union 94 (45) (2013) 409–410, ISSN 2324-9250, doi:

\bibinfo{doi}{10.1002/2013EO450001}, URL http://onlinelibrary.wiley.com/doi/10.1002/2013EO450001/abstract.

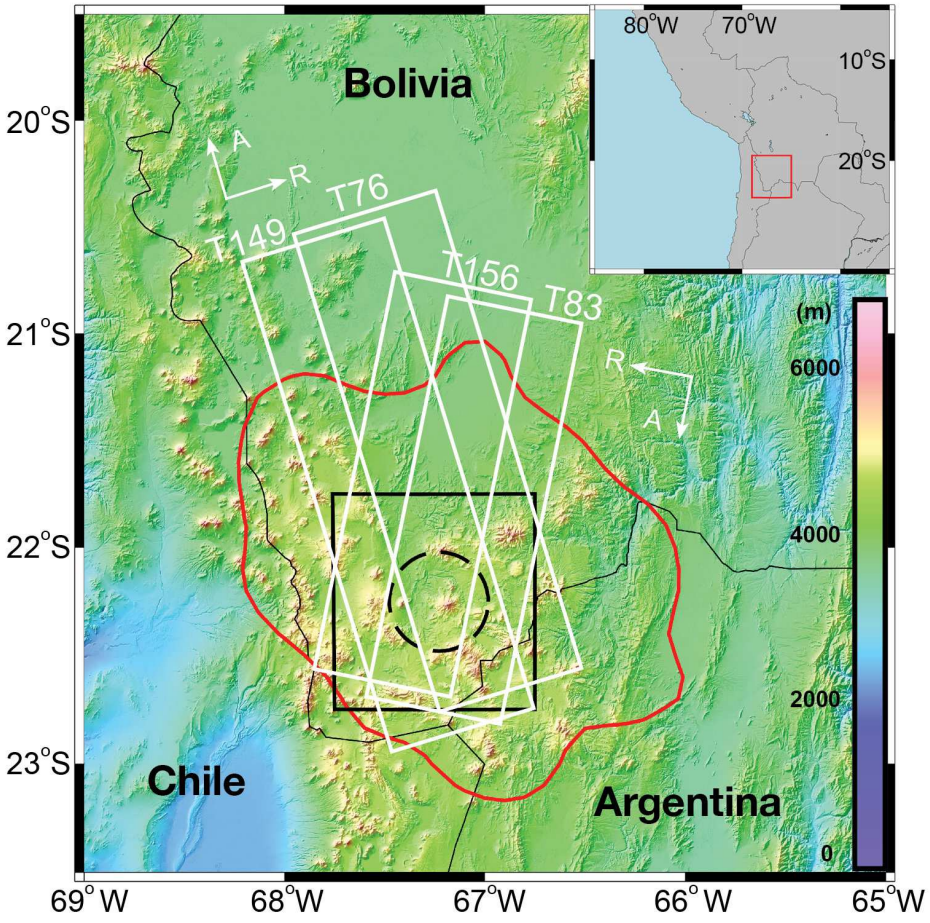

Figure 1: Overview map of area of interest. Sub-swathes of Sentinel-1 data from ascending (76, 149) and descending (83, 156) tracks used in this study are denoted by white rectangles. Arrows denote satellite heading (azimuth, A) and line of sight (range, R) directions. Black dashed circle represents the spatial extent of uplift documented by previous studies (Fialko and Pearse 2012; Henderson and Pritchard 2013). Red line denotes the 2.9 km/s velocity contour outlining the seismically imaged extent of the low velocity zone at depth of 20 km (Ward et al. 2017). Black rectangle denotes area shown in Figure 2.

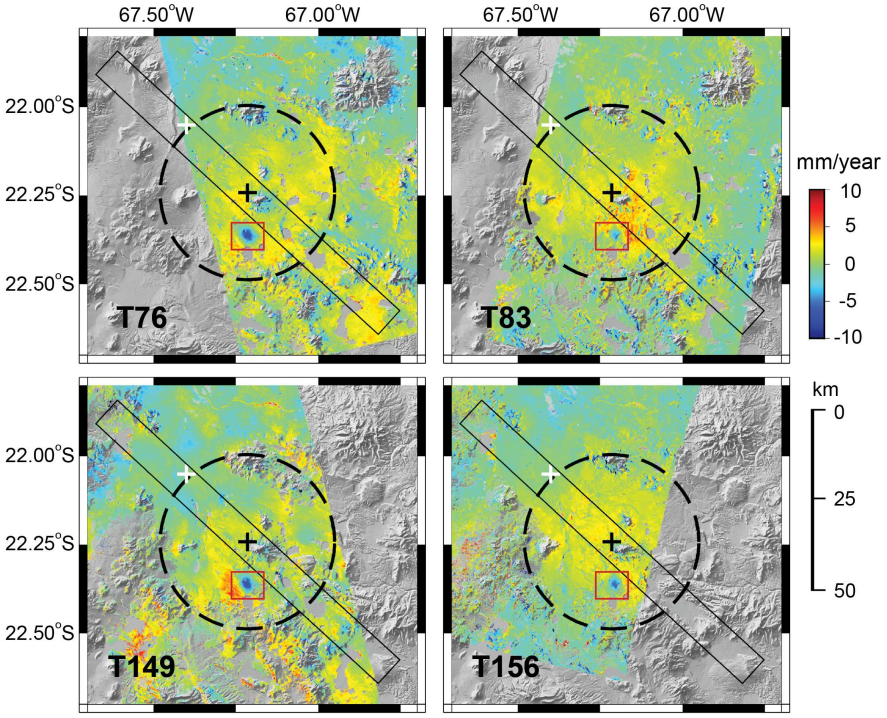

Figure 2: Mean LOS velocities for Sentinel-1 tracks 76, 83, 149 and 156. Positive velocities correspond to surface motion toward the satellite. Black dashed circle outlines an uplift observed between 1992-2010. Black solid rectangles denote a profile shown in Figure 3. White cross denotes a reference point for timeseries shown in Figures 4 and S4. Red rectangle outlines an area of local subsidence.

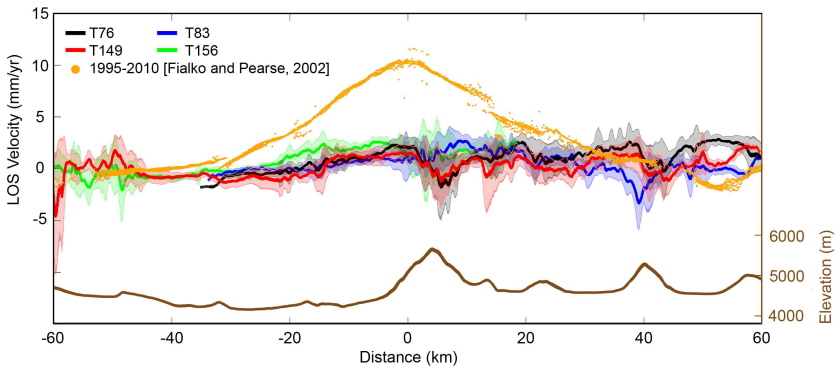

Figure 3: LOS velocities from the 10 km-wide northwest-southeast profile (see Figure 2) from 4 Sentinel-1 tracks: 76 (black), 83 (blue), 149 (red) and 156 (green). Shaded areas represent data within one standard deviation using a 500 m moving-average window. The average LOS velocities from the 1995-2010 epoch (Fialko and Pearse 2012) are shown by orange dots for comparison. Brown dots denote variations in topography along the same profile.

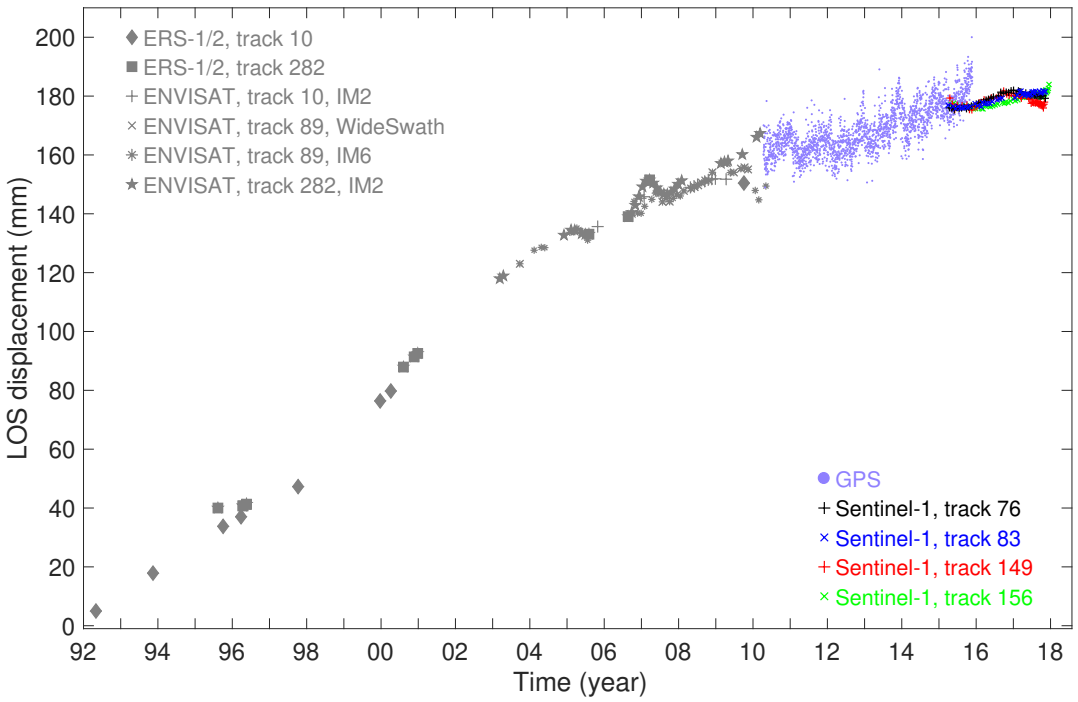

Figure 4: Combined timeseries of uplift from ERS-1/2 and ENVISAT (gray symbols, Fialko and Pearse 2012), continuous GPS (purple dots, Gottsmann et al. 2017b), and Sentinel-1 (color symbols, this study) observations. GPS data are projected onto the average line of sight of Sentinel-1. InSAR timeseries exhibit smaller seasonal variations compared to the GPS timeseries due to a relative nature of InSAR measurements (with respect to a nearby reference point) and atmospheric corrections.

Supporting Information for

"Variations in the Long-term Uplift Rate at Uturuncu Due to the Altiplano-Puna Magma Body Observed with Sentinel-1 Interferometry"

Homan Lau[1], **Ekaterina Tymofyeyeva**[1], **Yuri Fialko**[1]

[1]Institute of Geophysics and Planetary Physics, Scripps Institution of Oceanography, University of California, San Diego, La Jolla, CA 92093, USA.

Contents

Corresponding author: Homan Lau, h4lau@ucsd.edu

Figures S1 - S4

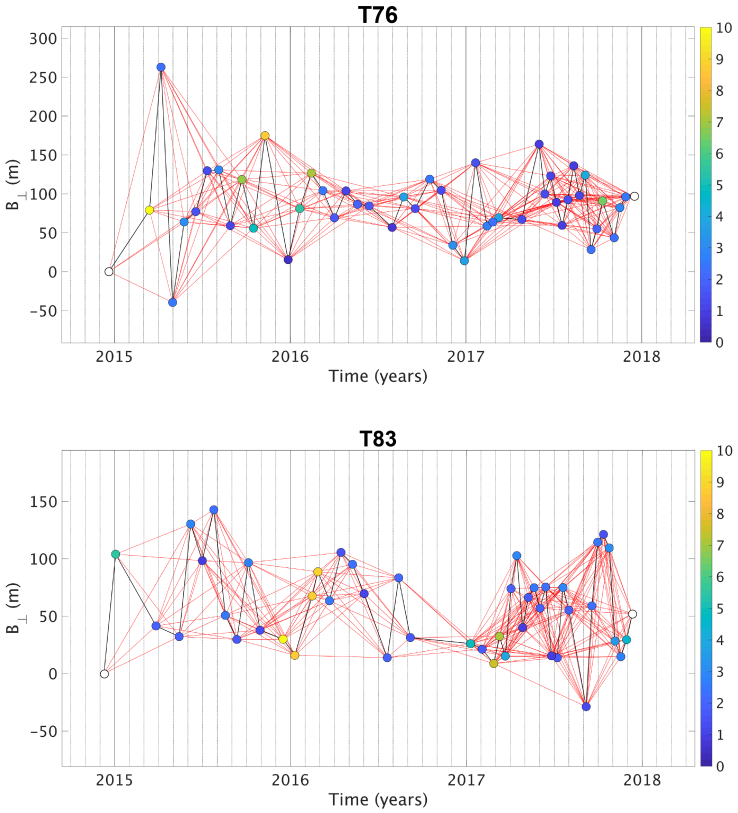

Figure S1. Perpendicular baselines for Sentinel-1 tracks 76 and 83. Color symbols denote the magnitude of atmospheric noise coefficients for each acquisition date; coefficients for the first and last SAR acquisitions are not computed. Black lines connecting the circles denote interferometric pairs. Red lines denote interferometric pairs that were used in estimation of atmospheric noise coefficients.

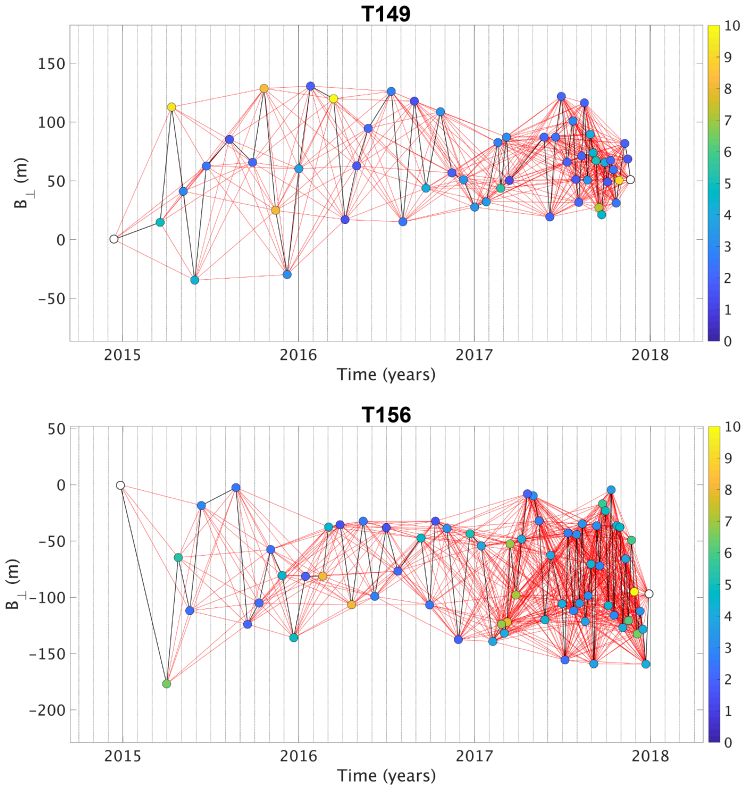

Figure S2. Perpendicular baselines for Sentinel-1 tracks 149 and 156. Notation is the same as in Figure S1.

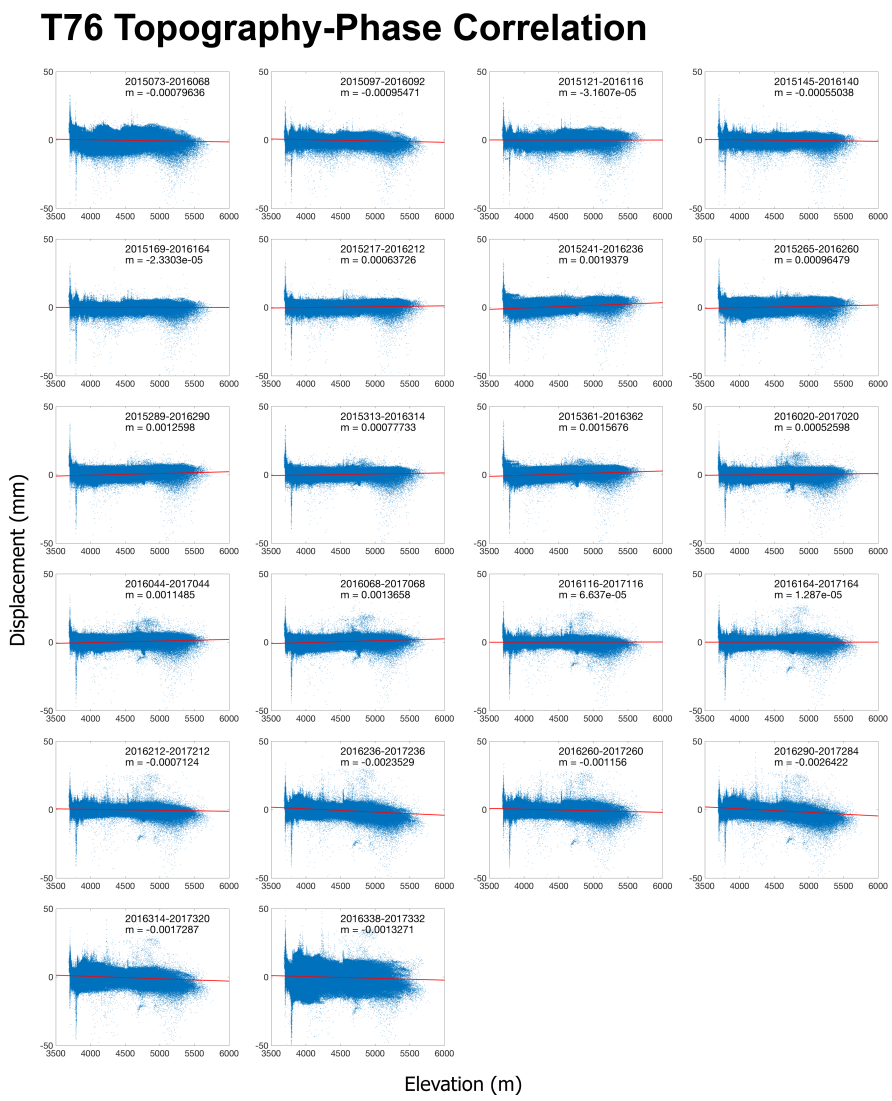

Figure S3. Correlation between topography and LOS displacements for year-long interferograms from Sentinel-1 track 76. Each interferogram we estimate the best linear fit between topography and LOS displacements using least squares. Blue dots denote the data and red lines denote the linear fit. The resulting parameters (the slope m and the intercept y of the best linear fit) are used to correct the interferograms for the effects of stratified atmosphere with

$$d_c = d_o - (m \cdot h + y), \tag{1}$$

where d_c are the corrected LOS displacements, d_o are input LOS displacements, and h is the local elevation at a given pixel.

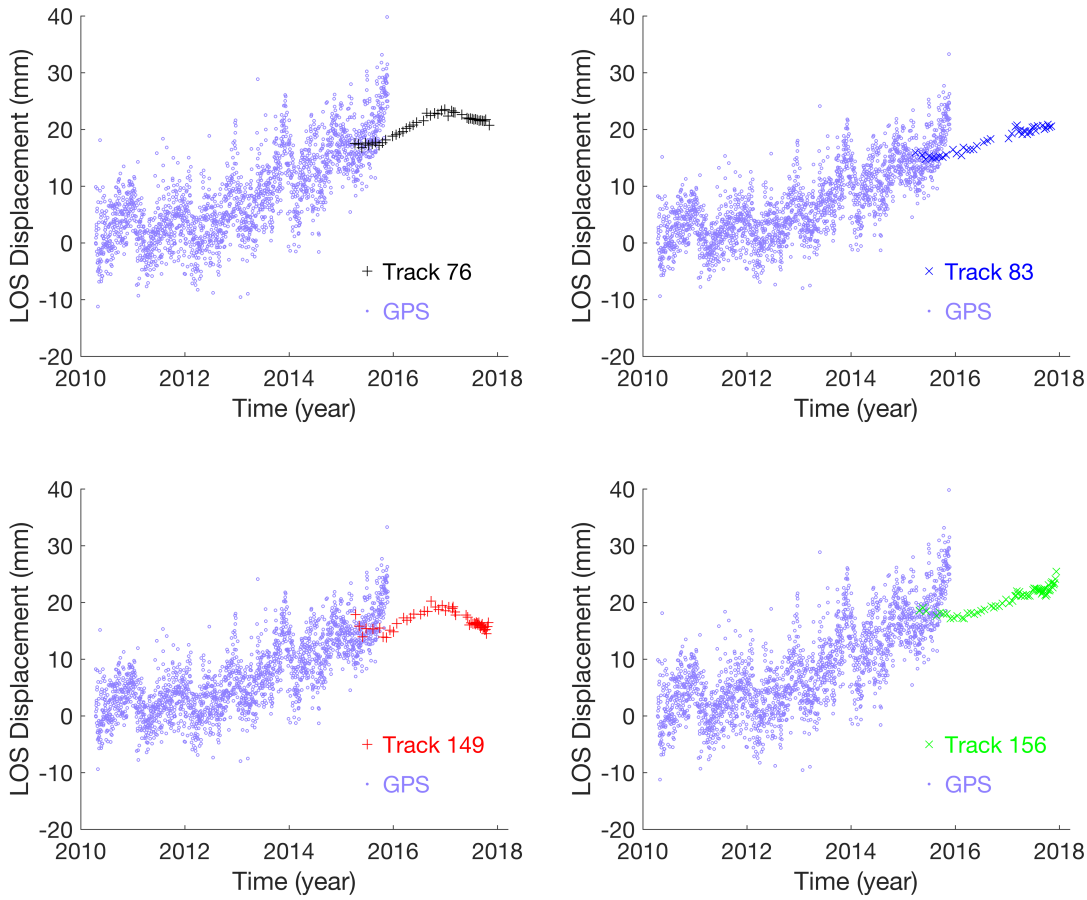

Figure S4. Time series of LOS displacements at the continuous GPS site UTUR for four Sentinel-1 tracks (color crosses). Purple dots denote the observed vertical GPS displacements projected onto the respective lines of sight. InSAR timeseries exhibit smaller seasonal variations compared to the GPS timeseries due to a relative nature of InSAR measurements (with respect to a nearby reference point) and atmospheric corrections.

Shallow deflation source

Mean LOS velocity data from all four satellite tracks show a localized negative anomaly (i.e., indicating subsidence) ~11 km south-southwest of Uturuncu's peak (outlined by a red square in Figure 2). The time series of LOS displacement indicate that subsidence occurred at a nearly constant rate over the last two years, with a peak rate of ~9 mm/year (Figure S5). The localized nature of subsidence is suggestive of a shallow source.

To estimate the source depth, we used a simple model of an isotropic volume change in a homogeneous elastic half-space [*Mogi* 1958]. We assumed a value of 0.25 for the Poisson's ratio of the host rocks, and inverted surface displacements for two model parameters, the source depth and volume change. Inversions were performed using iteratively re-weighted Levenberg-Marquardt least squares [*Holland and Welsch* 1977] with bisquare weight function to limit the influence of outliers, mostly due to atmospheric phase delays, at the peripheral region away from the deformation signal. We jointly inverted the mean LOS velocities from the four tracks, taking into account different look vectors and variations in incidence angle in range. The best-fit model, shown in Figure S6, suggests the source depth of 2.12 km and a volume change of 1.96×10^{-4} km^3/year.

Figures S5 - S6

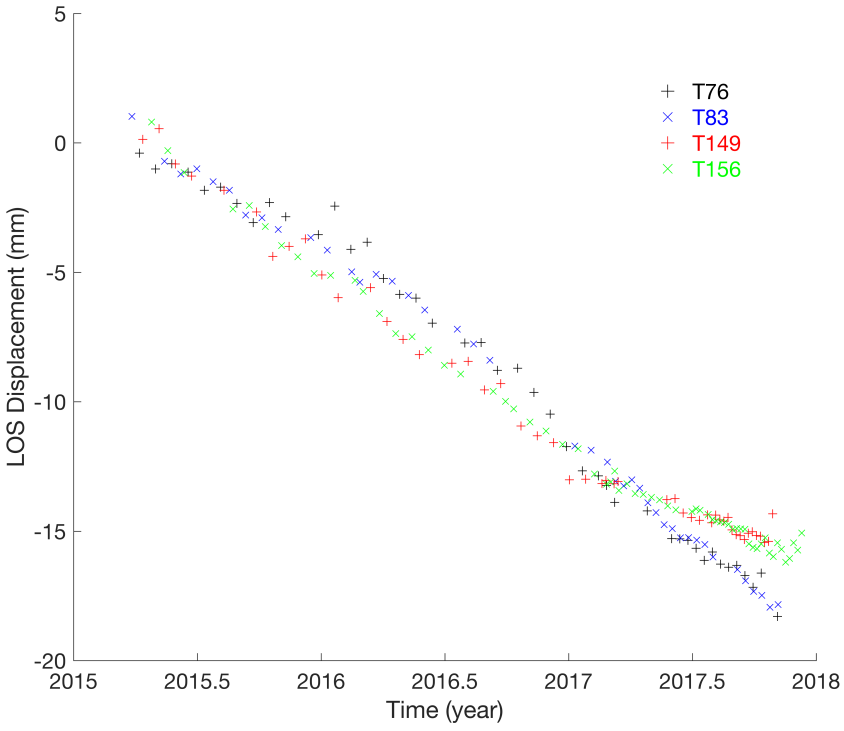

Figure S5. Timeseries of LOS displacements due to subsidence south-southwest of Uturuncu (see Figure 2). Symbols of different colors correspond to data from different Sentinel-1 tracks.

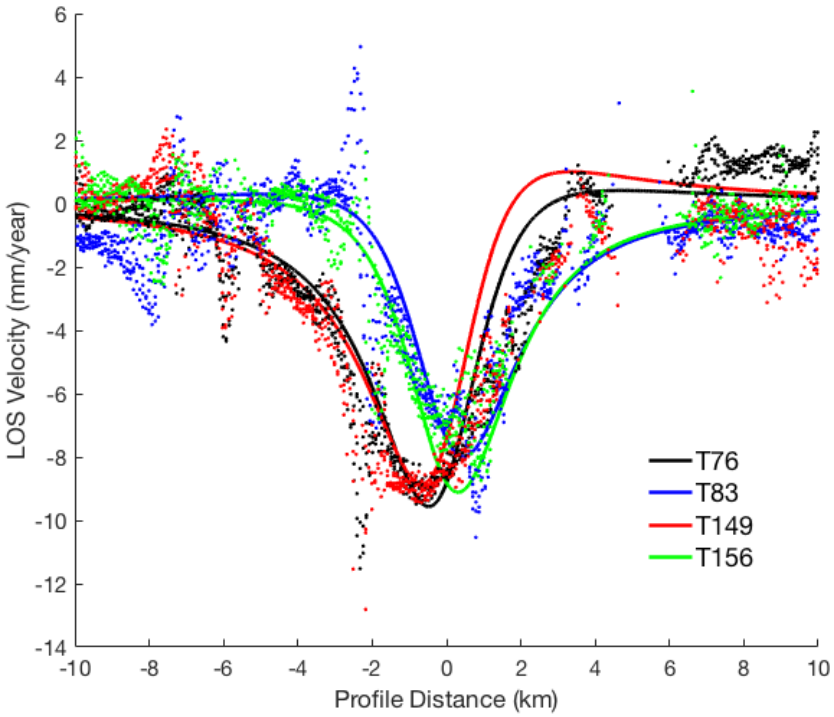

Figure S6. Observed (color dots) and modeled (color lines) mean LOS velocities from a profile across the subsidence area south-southwest of Uturuncu. The modeled velocities are from a joint inversion of data from all four InSAR tracks; different model predictions correspond to different incidence angles.

References

Holland, P. W., and R. E. Welsch (1977), Robust regression using iteratively reweighted least-squares, *Communications in Statistics - Theory and Methods*, *6*(9), 813–827, doi: 10.1080/03610927708827533.

Mogi, K. (1958), Relations between the eruptions of various volcanoes and the deformations of the ground surfaces around them, *Bull. Earthquake Res. Inst. Univ. Tokyo*, *36*, 99–134.